MAGNETOHYDRODYNAMICS Vol. 51 (2015), No. 2, pp. 225–235

OPTIMAL LINEAR PERTURBATIONS IN HARTMANN CHANNEL FLOW: THE INFLUENCE OF WALLS AND MAGNETIC DAMPING

S. Dong[1], *D. Krasnov*[2], *T. Boeck*[2]

[1] *Department of Power Engineering, North China Electric Power University, 071003 Baoding, China*

[2] *Institute of Thermodynamics and Fluid Mechanics, Ilmenau University of Technology, P.O.Box 100565, 98684 Ilmenau,Germany*

The transient amplification of optimal linear perturbations in Hartmann channel flow is studied at low and moderate Hartmann numbers. These perturbations are streamwise-independent vortices. They develop into streaks, which are important for subcritical transition to turbulence. The influence of the opposite channel wall is examined by comparing antisymmetric and symmetric perturbations. Differences in energy amplification between these two types of perturbations decrease rapidly with the Hartmann number. Moreover, the energy amplification in Hartmann flow is close to that in an asymptotic suction boundary layer, i.e. the magnetic damping of perturbations has only a weak effect on transient growth.

1. Introduction. When an incompressible and electrically conducting liquid flows between two unbounded parallel plates exposed to a uniform and constant magnetic field imposed perpendicular to the walls, the profile of the mean flow becomes flat in the core due to the interaction of the induced electric current with the imposed magnetic field. As a consequence, two boundary layers develop at the walls. They are named after Julius Hartmann [1], who first investigated MHD channel flow in 1937. The thickness of these layers is inversely proportional to the intensity of the magnetic field B, which is characterized by a non-dimensional parameter called the Hartmann number Ha. When Ha is sufficiently large, the Hartmann layers at the top and bottom walls do not overlap and can be considered as independent of each other. An isolated Hartmann layer could become unstable when the local Reynolds number R, which is defined with the Hartmann layer thicknessas length scale, exceeds some threshold.

The stability of Hartmann layers has been explored experimentally in laminarization studies to determine at which values of R_c turbulent flow becomes laminar. Early works showed that re-laminarization might occur in the range $150 < \mathrm{R}_c < 250$. A recent experiment [2] found $\mathrm{R}_c \sim 380$ from measurements of the friction coefficient as a function of R. The same R_c was observed for the inverse process of transition from laminar flow to turbulence.

The stability of Hartmann layers was first studied theoretically by normal mode analysis. It turned out that exponential growth of infinitesimal perturbations appears at values of R two orders of magnitude higher than $\mathrm{R_c}$ in experiments [3]. This is similar to other shear flows, e.g., pipe flow, where classical normal mode stability analysis fails to predict the transition. Recent developments in linear stability theory have revealed that the transient amplification of non-modal perturbations may play a significant role in the so-called subcritical transition of shear flows [4]. For a plane channel flow, streamwise vortices provide the strongest amplification. Such streamwise vortices interact with the mean flow and evolve into streamwise streaks, which are viewed as a key element in the transition scenario and in the dynamic processes sustaining turbulence. However, as

the subcritical transition is an intrinsically nonlinear process, the investigation of linear effects alone is insufficient to obtain critical parameters. In a non-magnetic shear flow, the transition Reynolds number $\mathrm{R_t}$ depends on the types of perturbations that are imposed on the laminar flow (transition scenario) as well as on their amplitudes, and direct numerical simulations (DNS) are required to determine, e.g., the dependence of $\mathrm{R_t}$ on the perturbation energy. For given perturbation energies, one may then estimate minimal values of R for transition from the values of $\mathrm{R_t}$ corresponding to the different scenarios. In plane channel flow, several scenarios have been explored, e.g., the interaction of oblique modes or the secondary instabilities of streaks [5].

In the Hartmann flow, the transient growth has been studied by Gerard–Varet [6] for an isolated Hartmann layer, where the opposite channel wall is neglected. The amplification of perturbations then depends only on R. Another study by Airiau and Castets [7] considered transient linear growth in the Hartmann flow with the full induction equation and explored the influence of Ha and the magnetic Prandtl number.

Krasnov *et al.* [8] examined a two-step transition scenario for the Hartmann flow by DNS. It consists of (i) the large transient growth of initially small, streamwise-independent disturbances that leads to a modulation of the laminar Hartmann flow, and (ii) the linear instability of the modulated flow with respect to some three-dimensional secondary perturbations. Transition could be triggered when both R and the amplitude of primary and secondary perturbations were sufficiently large. In this way, $\mathrm{R_c}$ was found to be between 350 and 400, which is already very close to the experimental results.

Further work by Zienicke and Krasnov [9] focused on the dependence of $\mathrm{R_c}$ on Ha in this scenario, i.e. the interaction between the Hartmann layers at both channel walls was taken into account. However, the effect of the channel walls on the primary streamwise-independent perturbations was not explored. This effect can be significant when the Hartmann layers are not small compared with the channel height. One purpose of the present paper is, therefore, to examine the linear optimal growth of streamwise-independent perturbations at low and moderate Hartmann numbers. In addition, the influence of the magnetic field on the amplification is investigated. The present study is thereby clearly limited to one aspect of the streak instability transition scenario, namely, the linear mechanism leading to the formation of streaks. The local transition Reynolds numbers R and the corresponding perturbation energies can only be determined by DNS using the linear perturbations (e.g., data from this study) as initial conditions of finite energy. The effects of walls and magnetic field on certain types of secondary perturbations of finite-amplitude streaks in the Hartmann flow will be examined in future work.

2. Governing equations. The flow of an incompressible electrically conducting fluid between two unbounded plates is considered in the inductionless approximation. The flow is driven by a constant mass flux and subjected to a constant and uniform magnetic field imposed perpendicularly to the walls. The non-dimensional governing equations and boundary conditions are

$$\frac{\partial \mathbf{u}}{\partial t} + (\mathbf{u}\cdot\nabla)\mathbf{u} = -\nabla p + \frac{1}{\mathrm{R}}\nabla^2\mathbf{u} + \frac{\mathrm{Ha}^2}{\mathrm{R}}\left(-\nabla\phi\times\mathbf{e}_z + (\mathbf{u}\times\mathbf{e}_z)\times\mathbf{e}_z\right), \tag{1}$$

$$\nabla\cdot\mathbf{u} = 0, \tag{2}$$

$$\nabla^2\phi = \nabla\cdot(\mathbf{u}\times\mathbf{e}_z), \tag{3}$$

$$u = v = w = \frac{\partial\phi}{\partial z} = 0 \quad \text{at} \quad z = \pm 1, \quad \text{periodicity in } x \text{ and } y \text{ directions.} \tag{4}$$

Here x, y, z denote the streamwise, spanwise and wall normal directions, respectively, and $\mathbf{e}_z \equiv (0,0,1)$. The center line velocity U of the laminar Hartmann flow, the half width of the channel L, and the imposed magnetic field strength B have been taken for non-dimensionlization. The non-dimensional parameters in the equations above are the Reynolds number $\mathrm{R} \equiv UL/\nu$ and the Hartmann number $\mathrm{Ha} = L/\delta$, where $\delta = \sqrt{(\rho\nu/\sigma B^2)}$ denotes the Hartmann layer thickness. The local Reynolds number is $\mathrm{Rl} = U\delta/\nu = \mathrm{R}/\mathrm{Ha}$.

For the analysis of primary perturbations, the governing equations (1)–(3) are linearized about the laminar Hartmann flow

$$\mathbf{U}(z) = \frac{\cosh(\mathrm{Ha}) - \cosh(\mathrm{Ha}\, z)}{\cosh(\mathrm{Ha}) - 1}\, U\, \mathbf{e}_x. \tag{5}$$

The primary linear perturbations take the form

$$\mathbf{u}_p(x,y,z,t) = \frac{1}{2}\left[\hat{\mathbf{u}}(z,t)\exp(i\alpha x + i\beta y) + \text{c.c.}\right], \tag{6}$$

where 'c.c.' denotes the complex conjugate. The stream- and spanwise wave numbers are denoted α and β. The growth of the perturbations is evaluated by the kinetic perturbation energy. An energy norm is defined as $E(t) = (1/2)\int |\mathbf{u}_p|^2 dV$, thus the ratio of $E(t)$ and initial perturbation energy $E(0)$ is the perturbation energy amplification factor $G(t) = E(t)/E(0)$.

Using a Lagrangian formalism, the maximum value $G_{\max}(\mathrm{R}, \mathrm{Ha}, \tau, \alpha, \beta)$ for the given parameters R, Ha, the wavenumbers α, β and a given time horizon τ is determined via an optimization with two constraints: (i) the perturbation energy $E(0) = 1$; (ii) the perturbation satisfies the linearized governing equations as well as the boundary conditions in the time interval $0 < t < \tau$. The Lagrangian multipliers, the so-called adjoint fields $\tilde{\mathbf{u}}(z,t)$, are introduced to enforce these constraints [4]. The optimal perturbation and amplification at the final time τ can be obtained by an iterative scheme, in which forward integration of the linearized governing equation is followed by backward integration of the adjoint equations, i.e.

$$\begin{array}{ccc} \hat{\mathbf{u}}(z,0) & \overset{direct}{\longrightarrow} & \hat{\mathbf{u}}(z,\tau) \\ \uparrow & & \downarrow \\ \tilde{\mathbf{u}}(z,0) & \overset{adjoint}{\longleftarrow} & \tilde{\mathbf{u}}(z,\tau). \end{array} \tag{7}$$

The relations between the fields at initial and final times are described, e.g., in [10]. The iterations can be stopped when the energy amplification factor G tends to a stationary value. We note that the pressure and electric potential as well as their adjoints are functions of the velocity fields and have no independent dynamics. The iterative method (7) for computing the optimal perturbations and the corresponding code are described in [11].

3. Influence of the opposite channel wall. Optimal linear growth in the Poiseuille flow without magnetic field has been analyzed by Butler and Farrell [12]. The largest energy amplifications are obtained for α=0 at sufficiently long times τ. Transient energy growth is then caused by a redistribution of streamwise velocity by streamwise-independent vortices (lift-up mechanism). The Poiseuille flow supports two classes of such perturbations with different vertical structures. With the increasing width of the plateau between the Hartmann layers, these perturbations should become localized at the walls. In this case, one should recover the results for optimal linear growth in an isolated Hartmann layer by Gerard–Varet [6].

3.1. Antisymmetric and symmetric perturbations. In the hydrodynamic case, the vertical perturbation structure of purely streamwise-independent perturbations (α=0) can be either antisymmetric or symmetric in z for the initial wall-normal velocity profile $\hat{w}(z,0)$, which results in a *symmetric* or an *antisymmetric* perturbation (with respect to the streamwise perturbation velocity). The quantity $\hat{w}$ will be assumed as real. The corresponding perturbation $\hat{u}$ of the streamwise velocity is complex.

As Butler and Farrell [12], we consider a fixed R = 5000. In addition, we vary the Hartmann number in order to see the localization of the perturbations and to determine when they become identical. This is possible because in the numerical method the antisymmetric or symmetric structure of perturbations is preserved from one iteration to the next.

When the Hartmann number is small, the basic velocity profile is close to the Poiseuille flow, and the two perturbations types should resemble those for Ha = 0. This is shown in Fig. 1 for Ha = 2 and R = 5000 for a minimal domain with a single spanwise wavelength. The top row shows the initial velocity distribution in a plane x = *const*. For the symmetric perturbations, one finds stacked pairs of counter-rotating vortices along the vertical direction and no flow across the mid-plane. For the antisymmetric perturbations, the vortices extend over the full height of the channel with weak co-rotating vortices near the middle. The

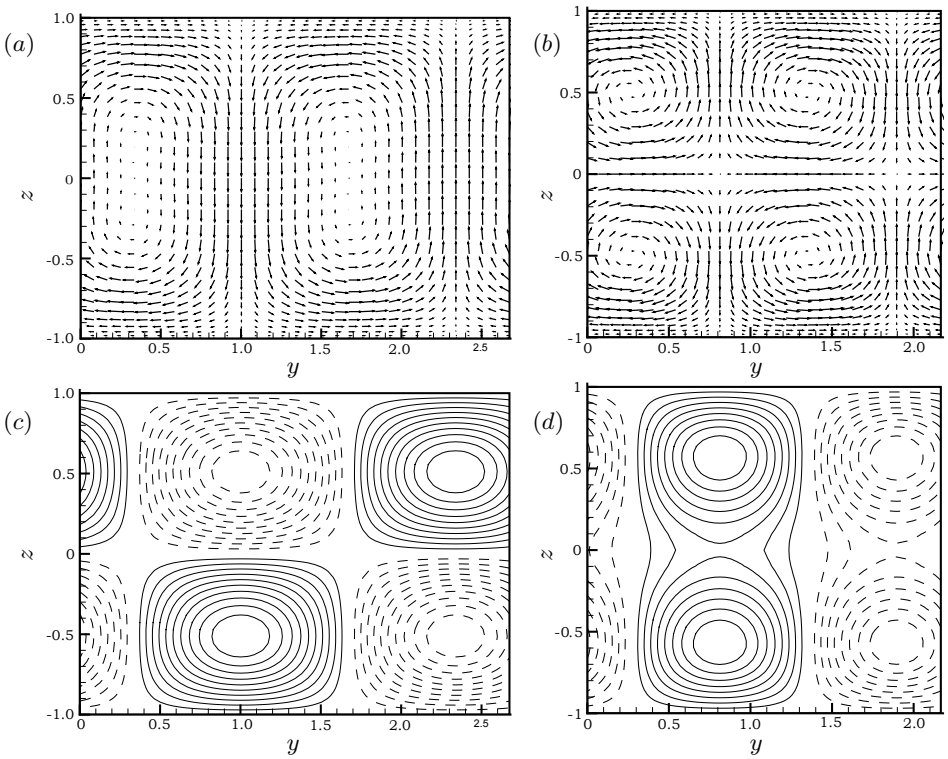

Fig. 1. Results for R = 5000 and Ha = 2: perturbation velocity distributions of a globally optimal antisymmetric perturbation (a, c) and a symmetric perturbation (b, d) in the (y,z)-plane. Top row (a, b) – the velocity distribution at the initial time; bottom row (c, d) – streamwise velocity contours at the time τ of maximum amplification. Dashed lines indicate negative values.

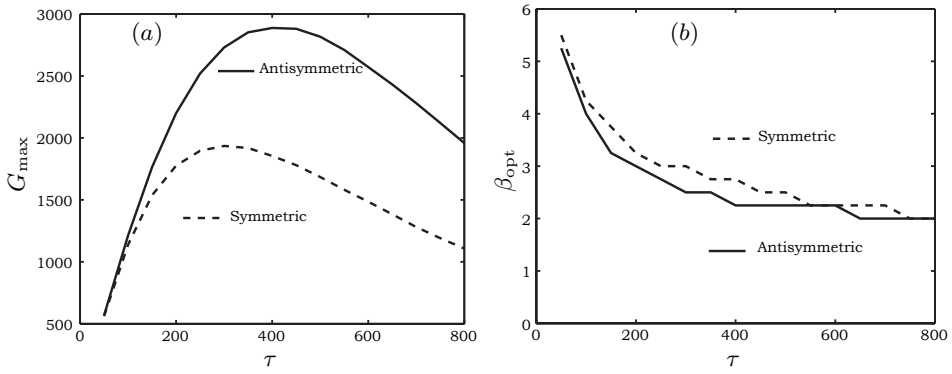

Fig. 2. Maximum of the perturbation energy amplification $G_{\max}$ (a) and the corresponding optimal spanwise wavenumber $\beta_{\rm opt}$ (b) as a function of the time horizon τ at R = 5000 and Ha = 2.

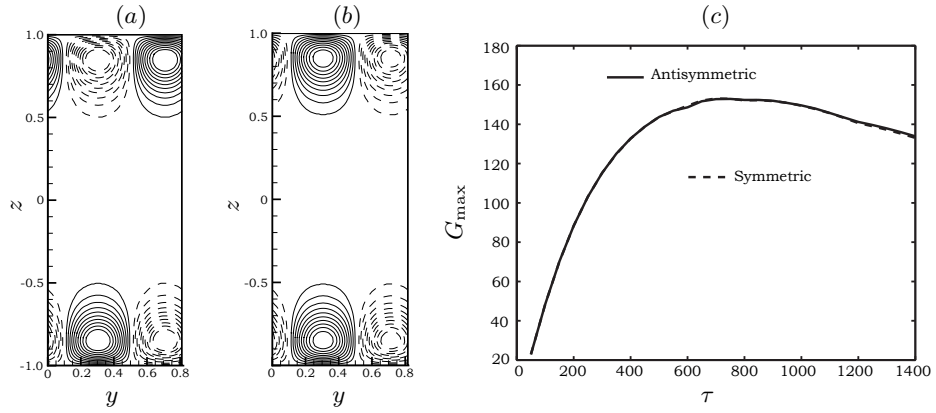

Fig. 3. Results for R = 5000 and Ha = 10: (a,b) Distribution of the streamwise perturbation velocity at the optimal time τ for antisymmetric (a) and symmetric (b) perturbations. (c) Maximum of the energy amplification $G_{\max}$ as a function of the time horizon τ.

resulting isolines of the streamwise velocity perturbation in Fig. 1 are symmetric and antisymmetric with respect to the mid-plane.

Fig. 2 shows that the maximum energy amplification $G_{\max}(\tau)$, i.e. the amplification factor G optimized with respect to β, is higher for the antisymmetric perturbations. The corresponding values $\beta_{\rm opt}(\tau)$ providing $G_{\max}(\tau)$ are lower. In both cases, the amplification is lower than at Ha = 0, where $G_{\max} \approx 4900$ ($\beta_{\rm opt} \approx 2.0$) for antisymmetric perturbations and $G_{\max} \approx 2800$ ($\beta_{\rm opt} \approx 2.6$) for symmetric perturbations. However, both the optimal times and the wave numbers hardly differ from Ha = 0.

The separation of the Hartmann layers at higher Ha eliminates the differences between symmetric and antisymmetric perturbations. This can be seen in Fig. 3 for Ha = 10. The streamwise velocity perturbations appear to have a very similar shape and show almost identical values $G_{\max}$ at essentially the same optimal time $\tau_{\rm opt}$ and wavenumber $\beta_{\rm opt}$. The energy amplification is also significantly reduced and occurs at a later time and for a higher wavenumber than at Ha = 2 (Fig. 3c).

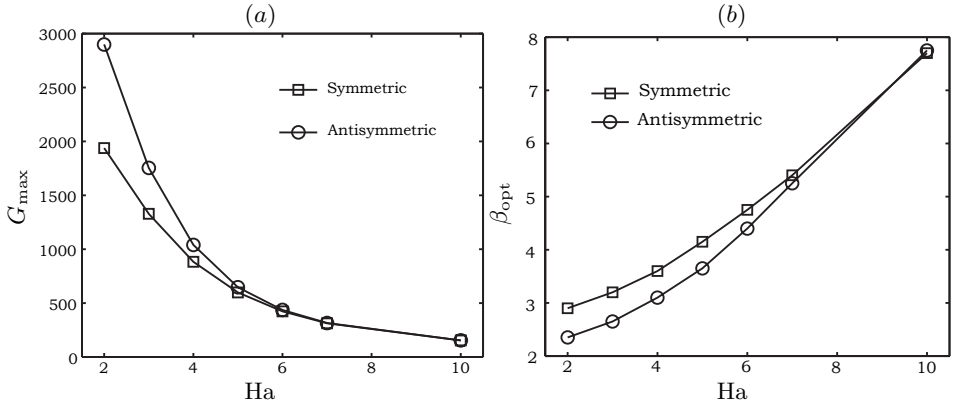

Fig. 4. Global maximum of the perturbation energy amplification $G_{\max}$ (a) and the corresponding optimal spanwise wavenumber $\beta_{\rm opt}$ (b) for different Ha at R = 5000.

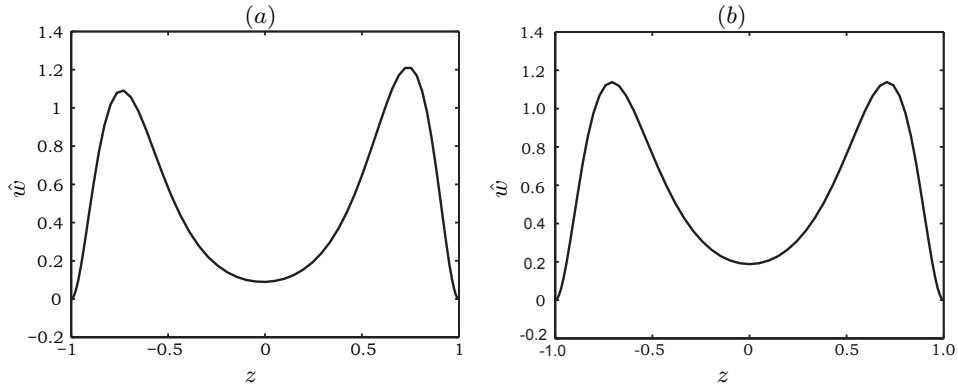

Fig. 5. Distribution of the vertical velocity $\hat{w}$ at R = 5000 and Ha = 7 after N = 5 (a) and N = 1155 (b) iterations. The wavenumber $\beta_{\rm opt}$ is that of the largest amplification of antisymmetric perturbations.

3.2. Convergence to the limit of an isolated Hartmann layer. A detailed exploration of the interval 2 < Ha < 10 was performed at R = 5000 to see how the different perturbation types approach one another. Fig. 4*a* shows how the maximum energy amplification of antisymmetric and symmetric optimal perturbations changes with Ha. The differences become insignificant for Ha > 7. The corresponding wavenumbers $\beta_{\rm opt}$ in Fig. 4*b* are then also fairly close. Moreover, they become proportional to Ha for Ha > 7, which also inidicates that the perturbations become localized within the Hartmann layers. Nevertheless, the effect of the opposite wall is not completely absent even then, i.e. the symmetric and antisymmetric perturbations are not exactly identical. The antisymmetric perturbations are still growing faster, but the differences appear to become exponentially small.

A direct computation of such small differences in amplification between the perturbations is hardly possible with our iterative numerical method. Instead, we use an indirect approach. When a general initial perturbation that is neither symmetric or antisymmetric is used in the iterative method, it will eventually converge to the antisymmetric perturbation with the larger amplification. However, the number of iterations will increase as the difference in amplification between the symmetric and antisymmetric perturbations decreases.

Fig. 5 shows two iterates of the vertical velocity perturbation $\hat{w}$ to illustrate the convergence from a random initial distribution. After N = 5 iterations the

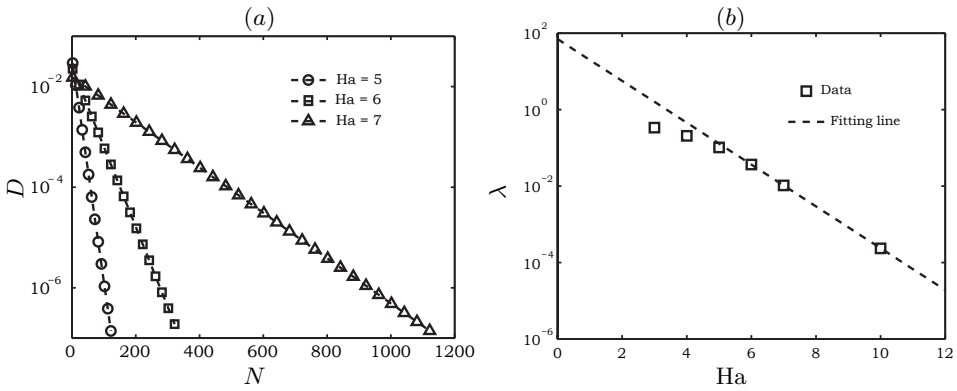

Fig. 6. R = 5000: (*a*) Convergence of D with the iteration number N at different Ha. (*b*) The decay rate coefficient λ as a function of Ha. In each case, the wavenumber β_{opt} is that of the largest amplification of antisymmetric perturbations.

profile is not symmetric about $z = 0$, but after $N = 1155$ it has essentially converged to a symmetric one, i.e. the antisymmetric perturbation is dominant.

To characterize the asymmetry of the $\hat{w}$ profile, a parameter D can be defined as the difference between the left peak and the right peak in $\hat{w}$ (see Fig. 5*a*), i.e.

$$D = \left| \max_{z>0}(\hat{w}(z)) - \max_{z<0}(\hat{w}(z)) \right|. \tag{8}$$

Its value decreases with the number of iterations N as the symmetric profile is approached. Fig. 6*a* shows that the convergence is exponential, i.e.

$$D(N) \sim \exp(-\lambda N). \tag{9}$$

The decay rate λ depends on the Hartmann number. Fig. 6*b* shows that it decreases rapidly with Ha. From Ha > 6, there appears to be an approximately exponential dependence, i.e. $\lambda \sim \exp(-C\text{Ha})$.

4. Magnetic damping effect on perturbations. In the laminar Hartmann flow, the flat velocity distribution in the bulk is caused by the balance between the induced Lorentz force density and the pressure gradient, and the resulting Hartmann layers are due to a balance of viscous and Lorentz forces. The ratio of Lorentz forces to inertia in the Hartmann layers is described by the magnetic interaction parameter N_δ based on the Hartmann layer width. According to Alboussiere and Lingwood [13], $N_\delta \sim \text{Ha/R}$, which is small when the Hartmann layer becomes turbulent. For this reason, these authors have argued that the turbulence in the Hartmann layer is essentially unaffected by the Lorentz forces, i.e. the Lorentz force is important only for the turbulent mean velocity, but not for the fluctuations. By the same argument, the Lorentz force should only have a weak effect on the optimal perturbations in the Hartmann flow. For a quantitative comparison, we shall, therefore, compute the evolution of optimal perturbations in the Hartmann flow with and without Lorentz forces. The results can also be compared with an asymptotic suction boundary layer (ASBL), which has the same mean velocity distribution as an isolated Hartmann layer, i.e.

$$U(z) = U\left(1 - \exp(-z'/\delta_S)\right), \tag{10}$$

where the boundary layer thickness $\delta_S = \nu/w_S$ depends on the suction velocity w_S and z' denotes the distance from the wall. Optimal growth in this flow has been

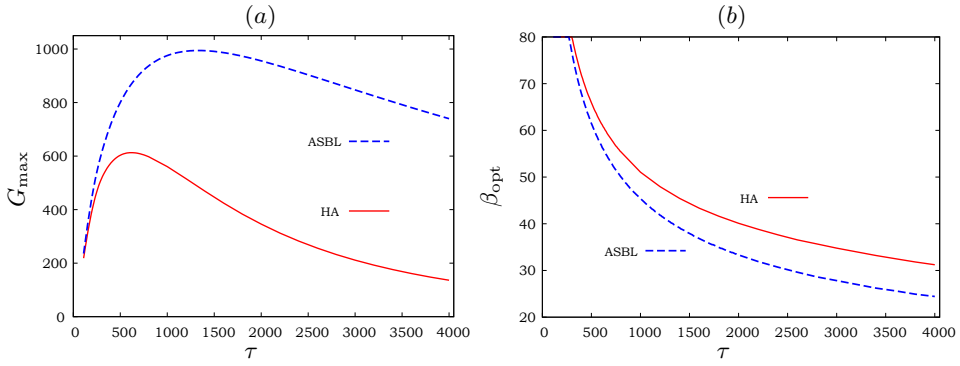

Fig. 7. Results at R = 1000 and Ha = 40: (*a*) The maximum energy amplification $G_{\max}$ and (*b*) the optimal spanwise wavenumber β_{opt} as a function of the time horizon τ for a full Hartmann flow (HA) and a Hartmann flow without magnetic damping (ASBL).

computed by Fransson and Corbett [14]. Incidentally, these authors found that the primary perturbations of the ASBL were not much affected by the suction, i.e. the amplification is largely the same when the vertical velocity at the wall is set to zero. The ASBL without suction velocity in the perturbation problem is then equivalent to an isolated Hartmann layer without magnetic field in the perturbation problem. For this reason, we loosely refer to the results at Ha = 0 by "ASBL" in what follows. In the ASBL, one can define a local Reynolds number based on the boundary layer thickness, i.e. $\mathrm{R} = U\delta_S/\nu$. It is equivalent to the local Reynolds number R for the Hartmann layer.

To compare the Hartmann flow (HA) and the ASBL, we have computed the optimal linear growth for streamwise-independent perturbations ($\alpha = 0$) at different Ha and R. The results for the maximum amplification G as a function of the time horizon τ and the corresponding wavenumber β, at which G is attained, are shown in Fig. 7 for Ha = 40 and R=1000. With small τ, the two cases are hardly different. However, for the ASBL there is a stronger amplification reached at a later time and a lower value of β since there is no Joule dissipation in this case. Time is shown as τHa, i.e. it is measured in convective units based on the boundary layer width. The values of β are high because β is represented with L

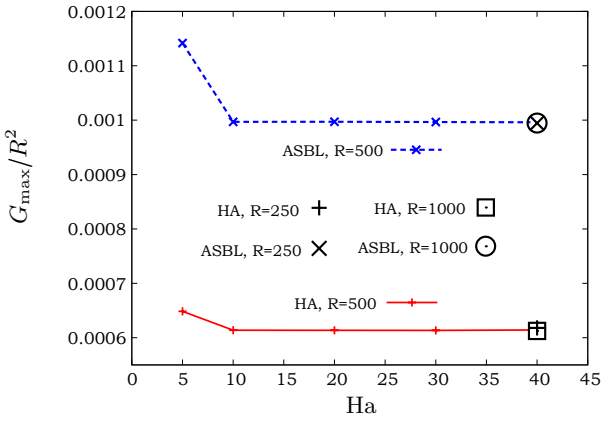

Fig. 8. Scaled global maximum of the energy amplification $G_{\max}$ for R = 500 (Ha = 5 . . . 40) and R = 250, 1000 (at Ha = 40).

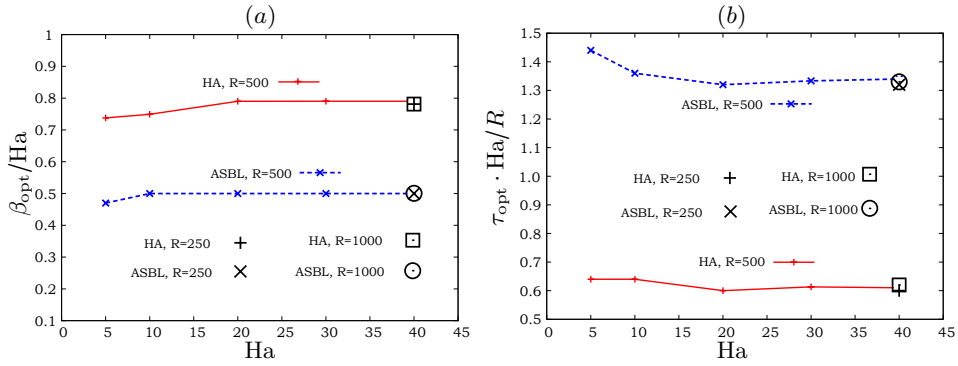

Fig. 9. Scaled optimal parameters corresponding to the global maximum of the energy amplification: (a) the spanwise wavenumber β_{opt} and (b) the time τ_{opt} for the cases of full Hartmann channel (HA) and ASBL.

Table 1. Values of the prefactors in Eq. (11) computed with the data for R = 1000 and Ha = 40. Data for the actual ASBL (with suction) and an isolated Hartmann layer are listed for comparison.

	C_G	C_τ	C_β
full Hartmann flow	6.1×10^{-4}	0.62	0.78
ASBL	9.9×10^{-4}	1.33	0.50
actual ASBL [14]	9.9×10^{-4}	1.15	0.53
Hartmann layer [6]	5.65×10^{-4}	n/a	0.9

as the unit of length.

We now consider the maximum energy amplification G_{max} optimized with respect to both τ and β. The corresponding values are τ_{opt} and β_{opt}, i.e. G_{max} is attained at these values. Since the local Reynolds number R is the essential parameter for an isolated Hartmann layer or ASBL, G_{max} as well as τ_{opt} and β_{opt} depend only on R when units of length, time and velocity are based on δ and on the velocity scale U. For the streamwise-independent perturbations, all these quantities exhibit distinct power-law dependences on R, which can be justified by an asymptotic analysis of the Orr–Sommerfeld and Squire equations [4, 6]. We, therefore, expect

$$G_{max} = C_G \mathrm{R}^2, \qquad \tau_{opt}\mathrm{Ha} = C_\tau \mathrm{R}, \qquad \beta_{opt}/\mathrm{Ha} = C_\beta. \tag{11}$$

Figs. 8 and 9 show that this scaling behavior indeed holds for different values of R and Ha when the Hartmann number is sufficiently large. The values of the different parameters are given in Table 1. The maximum amplification and the optimal time are smaller by about 1/2 for the Hartmann case in comparison with the ASBL. The optimal wavenumber is about 50% higher. Although the quantitative differences are not insignificant, the transient growth of optimal perturbations with and without magnetic field is fairly similar. Therefore, the flow stability appears to be mainly dependent on the mean flow profile.

We finally remark that the values for the prefactors of the Hartmann flow are somewhat larger than reported by Gerard–Varet. One may attribute the difference to an improved resolution of the wavenumber range.

5. Conclusions. The transient amplification of primary linear perturbations in a Hartmann channel flow at low and moderate Hartmann numbers has been

investigated in this study. Optimal primary perturbations of different vertical symmetry, i.e. antisymmetric and symmetric ones, have been considered to determine a possible interaction between opposite Hartmann layers. This was not addressed in [7], where only the global optimal perturbations, i.e. the antisymmetric ones, where considered. The antisymmetric perturbation is less stable than its counterpart, i.e. a higher energy amplification will be achieved at small Hartmann numbers in agreement with non-MHD channel flow. The difference in energy amplification between the antisymmetric and symmetric perturbations decreases rapidly with the Hartmann number, and at $Ha = 7$ the two layers can be viewed as isolated and non-interacting layers.

The convergence to the antisymmetric perturbation has been investigated by iterating from initial random perturbations. More iterations are necessary to approximate the antisymmetric perturbation solution at a large Hartmann number, though the amplification factor may not change significantly. The convergence rate has a simple exponential relationship with the Hartmann number.

Finally, we notice that the magnetic damping of perturbations is fairly weak, which is also suggested by the simulations of turbulent Hartmann flow [15]. As a result, the energy amplification in the Hartmann flow turned out to be close to that in an asymptotic suction boundary layer. For this reason, the transition to turbulence in the Hartmann flow should resemble that in an asymptotic suction boundary layer. A comparison between the Hartmann flow and the ASBL concerning the growth of secondary perturbations on boundary layer streaks is the subject of ongoing work.

Acknowledgments. TB, DK acknowledge the financial support from the Helmholtz Alliance "Liquid Metal Technologies". SD's work is supported by the National Natural Science Foundation of China (No. 11302076), the Natural Science Foundation of Hebei Province (No. A2014502047) and the Fundamental Research Funds for the Central Universities (No. 2014MS111).

REFERENCES

[1] J. Hartmann and F. Lazarus. Experimental investigations on the flow of mercury in a homogeneous magnetic field. K. Dan. Vidensk. Selsk. Mat. Fys. Medd. 15 (1937) 1–45.

[2] P. Moresco and T. Alboussière. Experimental study of the instability of the Hartmann layer. J. Fluid Mech., 504 (2004) 167–181.

[3] R.J. Lingwood and T. Alboussière. On the stability of the Hartmann layer. Phys. Fluids 11 (1999) 2058–2068.

[4] P.J. Schmid and D.S. Henningson. Stability and Transition in Shear Flows. (Springer 2001).

[5] S.C. Reddy, P.J. Schmid, J.S. Baggett and D.S. Henningson. On stability of streamwise streaks and transition thresholds in plane channel flows. J. Fluid Mech. 365 (1998), 269–303.

[6] D. Gerard-Varet. Amplification of small perturbations in a Hartmann layer. Phys. Fluids 14 (2002) 1458–1467.

[7] C. Airiau and M. Castets. On the amplification of small disturbances in a channel flow with normal magnetic field. Phys. Fluids 16 (2004) 2991–3005.

[8] D. Krasnov,E. Zienicke, O. Zikanov, T. Boeck and A. Thess. Numerical study of the instability of the Hartmann layer. J. Fluid Mech. 504 (2004) 183–211.

[9] E.A. Zienicke and D. Krasnov. Parametric study of streak breakdown mechanism in Hartmann flow. Phys. Fluids 17 (2005) 114101.

[10] S. Dong, D. Krasnov and T. Boeck. Secondary energy growth and turbulence suppression in conducting channel flow with streamwise magnetic field. Phys. Fluids 24 (2012) 074101.

[11] D. Krasnov, M. Rossi, O. Zikanov and T. Boeck. Optimal growth and transition to turbulence in channel flow with spanwise magnetic field. J. Fluid Mech. 596 (2008), 73–101.

[12] K.M. Butler and B.F. Farrell. Three-dimensional optimal perturbations in viscous shear flow. Phys. Fluids A 4 (1992) 1637–1650.

[13] T. Alboussière and R.J. Lingwood. A model for the turbulent Hartmann layer. Phys. Fluids 12 (2000) 1535–1543.

[14] J.H.M. Fransson and P. Corbett. Optimal linear growth in the asymptotic suction boundary layer. Eur. J. Mech. B-Fluids 22 (2003) 259–270.

[15] T. Boeck, D. Krasnov and E. Zienicke. Numerical study of turbulent magnetohydrodynamic channel flow. J. Fluid Mech. 572 (2007), 179–188.

Received 25.01.2015